

# Planner3D: LLM-enhanced graph prior meets 3D indoor scene explicit regularization

Yao Wei, Martin Renqiang Min, George Vosselman, Li Erran Li, Michael Ying Yang

**Abstract**—Compositional 3D scene synthesis has diverse applications across a spectrum of industries such as robotics, films, and video games, as it closely mirrors the complexity of real-world multi-object environments. Conventional works typically employ shape retrieval based frameworks which naturally suffer from limited shape diversity. Recent progresses have been made in object shape generation with generative models such as diffusion models, which increases the shape fidelity. However, these approaches separately treat 3D shape generation and layout generation. The synthesized scenes are usually hampered by layout collision, which suggests that the scene-level fidelity is still under-explored. In this paper, we aim at generating realistic and reasonable 3D indoor scenes from scene graph. To enrich the priors of the given scene graph inputs, large language model is utilized to aggregate the global-wise features with local node-wise and edge-wise features. With a unified graph encoder, graph features are extracted to guide joint layout-shape generation. Additional regularization is introduced to explicitly constrain the produced 3D layouts. Benchmarked on the SG-FRONT dataset, our method achieves better 3D scene synthesis, especially in terms of scene-level fidelity. The source code will be released after publication.

**Index Terms**—3D indoor scene synthesis, generative model, scene graph, large language model, spatial arrangement, latent diffusion.



## 1 INTRODUCTION

GENERATIVE models [1]–[4] have shown great potential in computer vision, natural language processing and multi-modal learning. With the learned patterns from generative models, data can be synthesized from scratch or other modalities. For controllable content creation, which has attracted increasing attention from both academia and industry, a variety of conditional generative methods have emerged on tasks such as text-to-image [5], [6], image-to-3D [7], [8] and text-to-3D [9], [10] generation. These cross-modal synthesis methods significantly reduce the data acquisition budget, especially for 3D content whose collection requires a lot of human efforts.

Despite the recent impressive breakthroughs in 3D content creation, most of the existing works [11]–[14] are restricted to single-object scenes, and their performance inevitably degrades on compositional scenes due to the limited understanding of object-object and scene-object relationships. Even trained on Internet-scale captioned 3D objects, for instance, Shap-E [9] struggles to reliably produce the results that are consistent with the given spatial or numerical prompts. Moreover, labor-intensive post-processing is essential to scale these approaches to complex scenes containing multiple objects, since the synthesized 3D shapes are sometimes in the non-canonical space.

In recent years, new pipelines capable of producing the entire 3D scenes have been developed using diverse inputs, such as LiDAR scans [15], single RGB images [16], captioned bounding boxes (i.e., scene layouts) [17] and scene

graphs [18]–[21]. As a semantic representation of 3D scenes, scene graphs provide a promising interface to control the generated 3D content, e.g., assigning properties to different instances of the same object category. However, 3D scene synthesis from scene graph is still at an early stage, and existing methods encounter various challenges.

Conventional works focus on scene layout generation regardless of 3D shape generation. Instead, the object shapes are retrieved from the existing shape databases. Though benefiting from reliable shape quality, as illustrated in Fig. 1 (a), it is hard for retrieval-based methods to generate coherent 3D scenes. For example, chairs appear in arbitrary shape styles. In addition, the performance heavily depends on the scale of the given databases. Differently, recent works synthesize the 3D scenes from generative perspectives. By category-specified shape decoders, semi-generative method Graph-to-3D [19] alleviates the limitation of retrieval-based method on shape consistency, but it suffers from low-quality shapes such as the incomplete wine cabinet shown in Fig. 1 (b). Fully-generative method CommonScenes [20] enables generative shape synthesis by adopting a latent diffusion model, which enhances the shape fidelity and diversity. Nevertheless, it can be seen from Fig. 1 (c) that the generated objects are spatially ambiguous due to the generated low-quality scene layouts. In fact, this frequently appears in (a), (b) and (c) where the table intersects the adjacent chair, denoted with red circles in the bottom-up views. These unrealistic scene generations leave a huge gap between previous methods and practical applications.

For controllable 3D scene synthesis, the generated objects should be not only realistic on its own but in harmony with the context of scene. To this end, we present **Planner3D**, LLM-enhanced grAph Prior meets 3D iNdoor scene Ne Explicit Regularization, for scene graph guided 3D scene synthesis. Instead of treating the compositional scene

- Yao Wei and George Vosselman are with University of Twente, The Netherlands.
- Martin Renqiang Min is with NEC Lab America, USA.
- Li Erran Li is with AWS AI, Amazon, USA.
- Michael Ying Yang is with Viusal Computing Group, University of Bath, UK. Email: [myy35@bath.ac.uk](mailto:myy35@bath.ac.uk).
- Project webpage: <https://sites.google.com/view/Planner3D/>

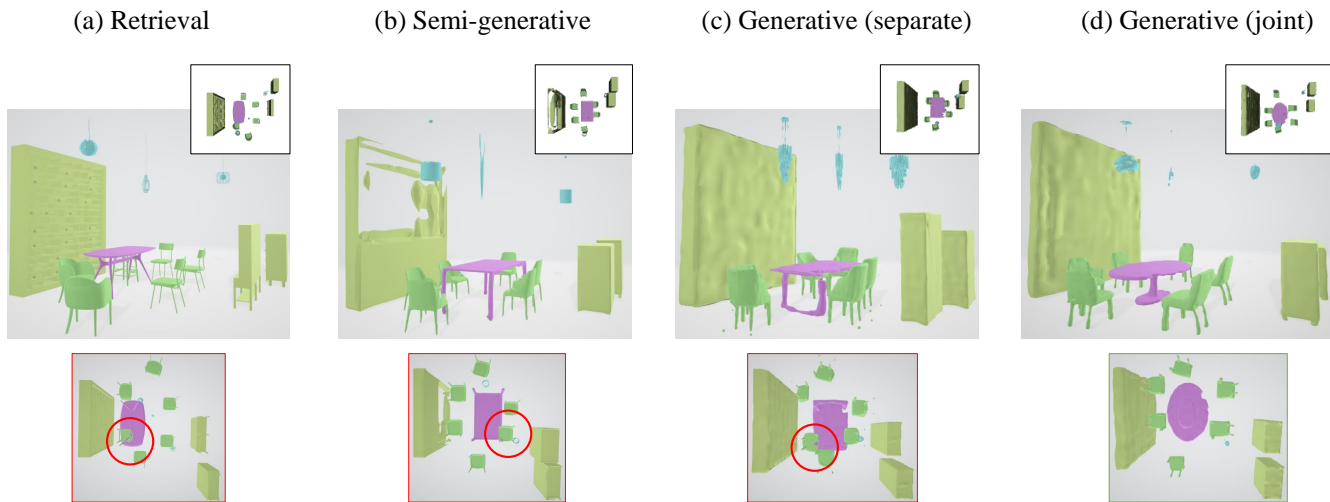


Fig. 1. Overview of previous works and ours. The 3D scenes are rendered from top-down view (top right), side view (middle), and bottom-up view (bottom). Unlike previous works that show poor shape consistency or spatial arrangements, Planner3D can synthesize higher-fidelity 3D scenes which demonstrate more realistic layout configuration while preserving shape consistency and diversity.

synthesis as two separate tasks, we work on joint layout-shape generation and explore controllable generative models by collaborating LLMs. Specifically, LLMs enhance the scene graph representation via interpreting the whole graph, which enables hierarchical understanding of the graph priors. Driven by a unified graph encoder, shape branch and layout branch are jointly trained to synthesize 3D scenes. Moreover, a layout regularization loss is introduced to explicitly encourage reasonable arrangements. As illustrated in Fig. 1 (d), our method is capable of generating realistic compositional 3D scenes. The **contributions** made in this work can be summarized as follows.

- We propose Planner3D, a controllable generative pipeline for compositional 3D indoor scene synthesis given scene graph. Planner3D effectively resolves the issues of unrealistic scenes and object collisions that plagued previous works.
- Scene graph prior enhancement mechanism is designed by adopting LLMs to produce global-wise textual representation from the graph, leading to hierarchical graph priors.
- A layout regularization loss, which explicitly constraints spatial arrangements and prevents unexpected intersections between objects, is introduced to a dual-branch graph-to-scene generation framework.
- Experimental results demonstrate that Planner3D improves the fidelity of scene synthesis. It attains 2.55 lower Fréchet Inception Distance (FID) score and 1.24 lower Kernel Inception Distance (KID) score compared to SOTA CommonScenes [20].

## 2 RELATED WORK

In this section, we discuss the most relevant literature on generative models for content creation, especially compositional 3D scene synthesis. We also survey emerging Large Language Models (LLMs) which are relevant to our work.

### 2.1 Generative models for content creation

Generative models have gained wide attention in recent years, with several prominent architectures emerging, including Variational Autoencoders (VAEs) [1], Generative Adversarial Networks (GANs) [2], Normalizing Flows (Flows) [3], and Denoising Diffusion Probabilistic Models (DDPMs) [4]. With the rapid improvements of deep learning techniques, these models are capable of creating novel content based on the learned distribution of training data. Using conditioning information, generative models can also be applied to personalized content creation, i.e., conditional generation. For example, taking natural language descriptions as the conditioning text prompts, there are many cross-modal applications, e.g., text-to-speech [26], [27], text-to-image [5], [6], text-to-video [22], [23], and text-to-3D [9], [10] synthesis. While remarkable progress has been made, challenges remain in conditional generation, particularly with regard to the controllability of generative models. Additionally, conditional generation lags behind in modalities such as 3D domain, due to the lack of large-scale datasets with high-quality condition-3D data pairs, and the complexity of modeling high-dimensional data.

For conditional 3D generation using generative models, most of the existing studies [9]–[14] primarily focus on synthesizing 3D scenes containing a single object. The object shapes are typically represented by explicit 3D representations that directly define the geometry of objects, such as voxel grids [29], point clouds [30], and meshes [31]. Multi-view images [33] are commonly used to capture the object’s appearance from various angles. Alternatively, some works employ implicit representations such as Signed Distance Functions (SDFs) [32] which model the 3D surfaces through continuous functions, and Neural Radiance Fields (NeRFs) [24] which model the volumetric scenes using neural networks. With the recent advances of 3D Gaussian Splatting [28], the hybrid explicit-and-implicit representation [25] is also explored. In this work, we use SDFs for geometry

representation which allows us to model multi-object scenes in a compositional manner.

## 2.2 Compositional 3D scene synthesis

Unlike object-centric 3D synthesis, multi-object 3D scene synthesis is more challenging where the object attributes (e.g., categories) and relationships become both crucial. Prior works [15]–[20] usually characterize a scene by spatial arrangements (i.e., layouts) and 3D shapes of the objects-of-interest within the scene. According to the styles of shape synthesis, these works can be broadly divided into three types of approaches.

**Retrieval based approaches.** For simplicity, conventional works [16], [18], [38], [46], [47] formulate the task as a combination of 3D layout prediction problem and 3D shape retrieval problem. They mainly concentrate on the former problem by training generative models to estimate 3D layouts given the input condition, such as scene graph [18], a single RGB image [16], and text prompts [46], [47]. The layouts are then populated with category-aware shapes to construct the 3D scenes. Specifically, the shapes are retrieved from the open-sourced databases, such as ShapeNet [34], 3D-FUTURE [35] and Objaverse [36], [37], based on euclidean distance of the bounding box dimensions [38]. However, this formulation depends heavily on the scale of the databases, suffering from limited shape diversity as well as inconsistent shapes of the same object category.

**Semi-generative approaches.** Concurrent studies [15], [17], [49] focus on generative shape synthesis, while scarifying the layout synthesis. Conditioned on LiDAR point clouds, XCube [15] can produce 3D scenes with high-quality meshes, though these partial observations are apparently not user-friendly inputs. Given axis-aligned 3D layouts that roughly provide the location and size of objects, Comp3D [17] is able to synthesize compositional 3D scenes that fit the specified object categories. CC3D [49] generates 3D scenes from 2D semantic layouts. While benefiting from extensive image data and 3D field representations, the results of layout-conditioned scene synthesis often exhibit view inconsistency problem. Also, these approaches impose strong geometric priors, significantly limiting the diversity of generated scenes. Graph-to-3D [19], a pioneering work in jointly shape and layout synthesis from scene graphs, overcomes the limitations of previous works in consistency and diversity. Nevertheless, its shape synthesis is bounded by pre-trained category-wise shape decoders.

**Fully-generative approaches.** Leveraging latent diffusion-based shape synthesis, CommonScenes [20] presents a fully-generative pipeline for 3D scene synthesis from scene graphs, achieving high-fidelity generation compared to previous studies. However, it suffers from three major issues. First, CommonScenes attempts to implicitly enrich scene graphs with contextual information which is restricted to individual edge-wise textual representations. The absence of global-wise explicit graph priors hinders effective feature extraction by graph convolution networks. Second, it struggles with generating coherent 3D scenes since the shape synthesis is isolated from the layout synthesis. Moreover, it mostly relies on adversarial training strategy for layout

synthesis, resulting in unrealistic layouts and object collisions. Motivated by addressing these problems, we involve LLMs for reasoning about the object-object and object-scene relationships from scene graphs. We also revisit the architecture and training scheme of 3D scene synthesis, especially in terms of graph encoder and layout decoder.

## 2.3 Annotations generated by LLMs

High quality labels play a vital role for machine learning (ML) systems. Traditionally, they are collected from humans manually or with limited ML assistance. Due to the high cost, large datasets with high quality text annotations are rare which hampers progress in the field. As LLMs are very capable, prior works have successfully employed LLMs to automatically generate annotations. In the NLP domain, besides earlier successes on generating annotations for tasks such as relevance detection, topic classification, and sentiment analysis, recently [39] shows GPT-4 can even generate data to solve advanced reasoning tasks. In the realm of images, LLMs are widely employed to generate question-answer text pairs from image captions for instruction tuning [40]–[42]. In video datasets, LLMs are primarily employed to enrich the text descriptions of videos. For instance, MAXI [43] leverages LLMs to generate additional textual descriptions of videos from their category names for training. InternVideo [44] utilizes LLMs to generate the action-level descriptions of videos from their frame-level captions. HowtoCap [45] leverages LLMs to enhance the detail in narrations of instructional videos. Lately, GraphDreamer [50] generates 3D scenes from texts by adopting LLMs to produce scene graphs as intermediate representations. LayoutGPT [48] regards LLMs as text-driven layout planners for scene synthesis. By contrast, we employ LLMs to generate global-wise textual descriptions of the scene graph. These rich and consistent descriptions prove to be vital to improve the representation learning in order to generate realistic compositional 3D scenes.

## 3 METHOD

Given a scene graph  $G$  describing the desired multi-object 3D scene using objects as nodes and their relationships as edges, Planner3D is able to synthesize realistic 3D scenes with consistent 3D object shapes and spatial layouts. As illustrated in Fig. 2, Planner3D consists of two main components: a scene graph prior enhancement mechanism and a dual-branch encoder-decoder architecture for graph-to-scene generation.

First, scene graph prior is enriched with LLM and vision-language model CLIP, and explicitly aggregates node-wise, edge-wise and global-wise textual representations of the input scene graph. The aggregated representation  $G^\dagger$  is fed to Graph Convolutional Networks (GCNs) and Multilayer Perceptron (MLP) layers, which are trained to model the posterior distribution of the 3D scene conditioned on the given scene graph. With the learned distribution  $Z$ , we update the node representation by replacing the original layout vector with the random vector  $z$  sampled from  $Z$ . Then, a graph encoder  $E_G$  learns to extract graph features from the updated graph representation  $G^\ddagger$ . A scene decoder takes

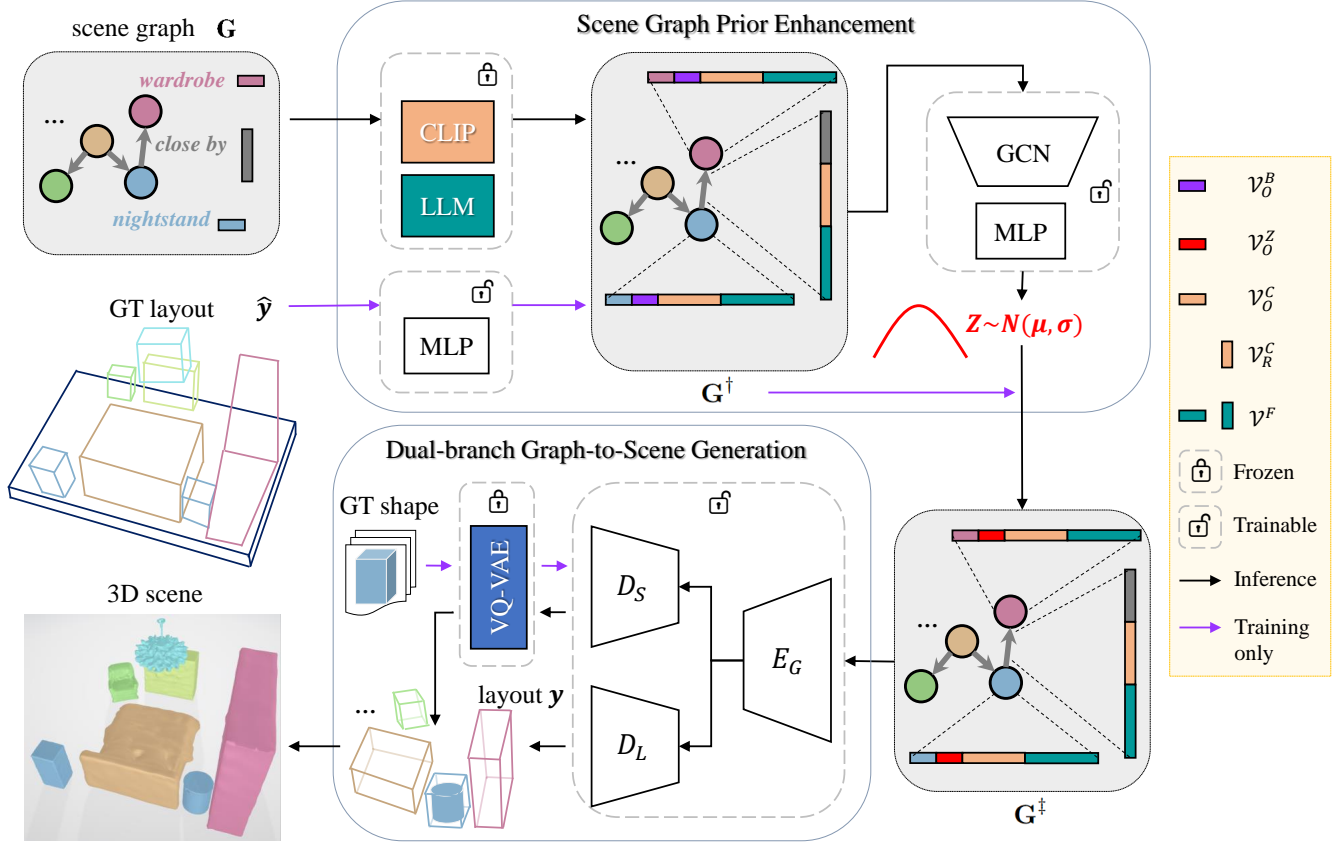


Fig. 2. Overview of Planner3D. Given a scene graph  $G$ , graph prior is enriched with LLM and CLIP to construct graph representation  $G^\dagger$ , which is then used to model the distribution  $Z$ . After updating graph node representation by replacing layout vectors with random vectors  $z$  sampled from  $Z$ , the updated graph representation  $G^\ddagger$  is input into the graph encoder  $E_G$ . Guided by the extracted graph features, consequently, the layout decoder  $D_L$  generates 7-parameterized layouts, and the shape decoder  $D_S$  works in conjunction with VQ-VAE to synthesize object shapes for graph nodes.

graph features as inputs and learns to generate 7-degrees-of-freedom 3D layout and shape latent through layout decoder  $D_L$  and shape decoder  $D_S$ , respectively. Compositional 3D scenes are eventually synthesized by fitting the generated layouts with the 3D shapes reconstructed from the shape latent by the pre-trained Vector Quantized Variational Autoencoder (VQ-VAE) decoder.

### 3.1 Scene Graph Prior Enhancement

The scene graph  $G = (O, R)$  typically consists of  $N$  nodes, i.e., objects  $O = \{o_1, o_2, \dots, o_N\}$ , and  $M$  directed edges, i.e., object relationships  $R = \{r_1, r_2, \dots, r_M\}$ . The representation of scene graph is initially composed of a set of feature vectors  $\mathcal{V}_O \in \mathbb{R}^{N \times Q}$  and  $\mathcal{V}_R \in \mathbb{R}^{M \times 2Q}$  for nodes and edges, which are embedded from the classes of objects  $O$  and relationships  $R$ , respectively.  $Q$  indicates the dimensions of feature vectors. Additionally, layout feature vectors  $\mathcal{V}_O^B \in \mathbb{R}^{N \times Q}$  are embedded using ground-truth (GT) layouts  $\hat{y}$  parameterized by 3D bounding box locations and sizes  $\hat{b}$  as well as angular rotations  $\hat{\alpha}$  along the vertical axis.

As demonstrated in Fig. 3(a), the pre-trained and frozen CLIP [51] is adopted to enrich the initial graph representation with inter-object insights. Specifically, nodes and edges are regarded as text prompts. Taking the objects  $o_i$  and  $o_j$  and their relationship  $r_{i \rightarrow j}$  as examples, we denote the corresponding relationship triplet  $\langle \text{subject, predicate, object} \rangle$

as  $\rho_{i \rightarrow j}$ , where  $o_i$ ,  $r_{i \rightarrow j}$  and  $o_j$  act as the subject, predicate, and object, respectively. CLIP text encoder is used to derive contextual feature vectors  $\mathcal{V}_{r_{ij}}^C \in \mathcal{V}_R^C$  for  $\rho_{i \rightarrow j}$ . Similarly, the vectors  $\mathcal{V}_{o_i}^C, \mathcal{V}_{o_j}^C \in \mathcal{V}_O^C$  are produced with prompts on subjects or objects of relationship triplets.

Furthermore, a pre-trained and frozen LLM is employed to generate feature vectors  $\mathcal{V}^F$  for the whole graph, enhancing the expressiveness of scene graph priors. By treating the scene graph as a set of relationship triplets  $\Omega = \{\rho_1, \rho_2, \dots, \rho_M\}$ , Instructor Transformer [52] which serves as LLM in this work, takes aggregated relationship triplets as input prompts and generates text embedding using an instruction with a format of "Represent the {DOMAIN} {TEXT-TYPE} for {TASK}". Here, we specify the instruction by Science, document and summarization, respectively. The resulting LLM-based vector  $\mathcal{V}^F$  is attached to each node and edge feature vectors.

Thanks to CLIP and LLM, the graph representation  $G^\dagger$  explicitly aggregates scene graph priors at the node-wise, edge-wise and global-wise levels. It can be formulated as,

$$G^\dagger = \{\mathcal{V}_O \circ \mathcal{V}_O^B \circ \mathcal{V}_O^C \circ \mathcal{V}^F, \mathcal{V}_R \circ \mathcal{V}_R^C \circ \mathcal{V}^F\}, \quad (1)$$

where  $\circ$  indicates the concatenation operation. Then, GCN layers are exploited to pass information along graph edges, followed by two MLP modules in parallel, each of which is composed of a MLP layer and additional two MLP

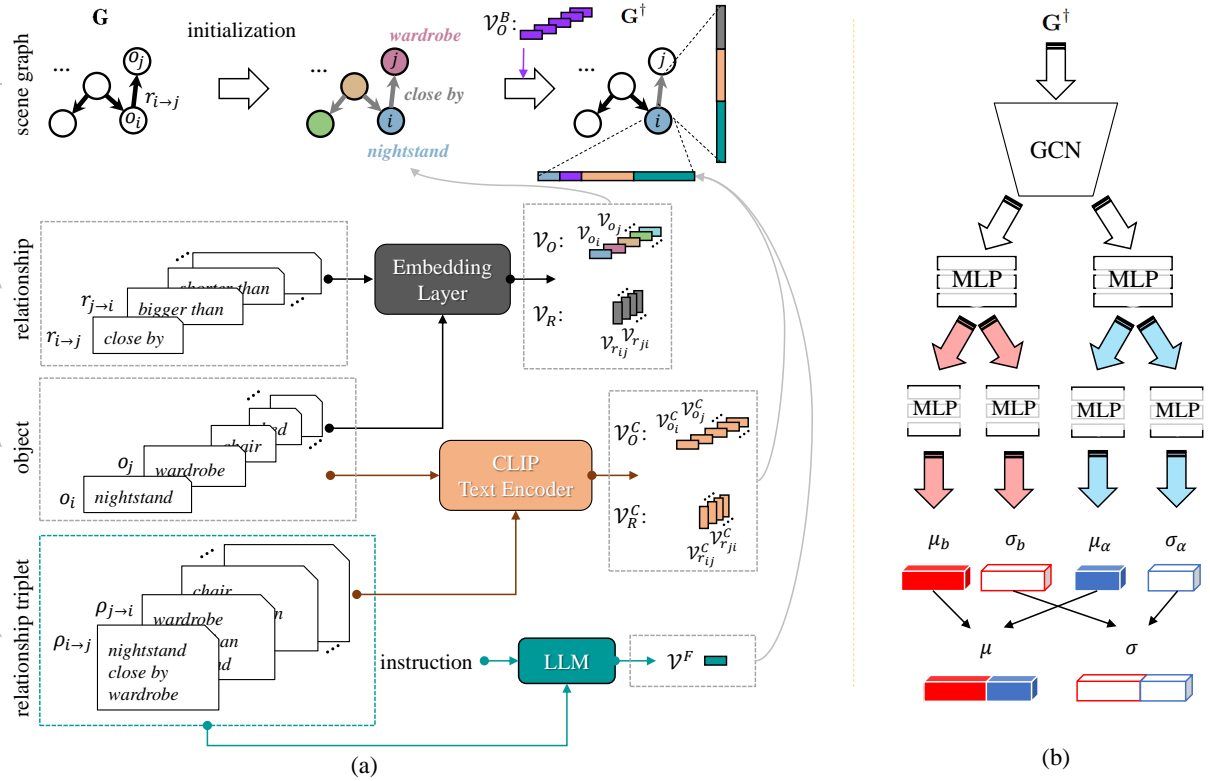


Fig. 3. Pipeline of scene graph prior enhancement. (a) Using CLIP and LLM, the graph representation  $G^\dagger$  explicitly aggregates node-wise, edge-wise and global-wise textual representations of the given scene graph. (b) The architecture of the model  $\phi$ , which learns to model the distribution  $Z \sim \mathcal{N}(\mu, \sigma)$  and is used to construct the graph representation  $G^\ddagger$ .

heads. Fig. 3(b) shows the architecture of GCNs and MLPs, parameterized as  $\phi$ . The MLP heads separately output the means (denoted as  $\mu_b$  and  $\mu_\alpha$ ) and the variances (denoted as  $\sigma_b$  and  $\sigma_\alpha$ ). By concatenating  $\mu_b$  and  $\mu_\alpha$  as well as  $\sigma_b$  and  $\sigma_\alpha$ ,  $\mu$  and  $\sigma$  are ultimately produced. Through reparameterization, random vectors  $z$  are sampled from the distribution  $Z \sim \mathcal{N}(\mu, \sigma)$  for each node. These random vectors  $\mathcal{V}_O^Z \in \mathbb{R}^{N \times Q}$  are utilized to replace the layout vectors  $\mathcal{V}_O^B$  that only work for the training phase. The updated graph is represented as follows,

$$G^\ddagger = \{\mathcal{V}_O \circ \mathcal{V}_O^Z \circ \mathcal{V}_O^C \circ \mathcal{V}^F, \mathcal{V}_R \circ \mathcal{V}_R^C \circ \mathcal{V}^F\}. \quad (2)$$

### 3.2 Dual-branch Graph-to-Scene Generation

The graph-to-scene architecture is composed of a graph encoder and a dual-branch scene decoder, shown in Fig. 4.

**Graph Encoder** Different from previous approaches that use two separate graph encoders to extract features for guiding the layout and shape decoders independently, we utilize GCNs layers as a unified graph encoder  $E_G$  for feature extraction from scene graph representation  $G^\ddagger$ . The shared graph features allow the following two decoders to interact with each other from an early stage. Note that  $E_G$  does not share parameters with the GCNs of  $\phi$  in the scene graph prior enhancement.

**Scene Decoder** The dual-branch decoder consists of a layout branch  $D_L$  which produces scene layouts for spatial

arrangements and a shape branch  $D_S$  which samples 3D object shapes for graph nodes. Specifically,  $D_L$  is achieved by two groups of stacked MLP layers in parallel. For the graph node  $i$ , one group of MLPs is leveraged to predict the 6-parameterized 3D bounding box  $b_i$  including width, length, height and centroid coordinates, and another group predicts the angular rotation  $\alpha_i$  along the vertical axis. It can be formulated by,

$$y = \{b \circ \alpha\} = D_L(E_G(G^\ddagger)). \quad (3)$$

In addition, the shape branch  $D_S$  is implemented by a group of stacked MLPs (denoted as  $\omega$  to distinguish them from the MLPs of the layout branch) and a conditional latent diffusion model. We utilize Truncated SDFs (TSDFs) [53] with resolution  $d_{SDF}$ , which can be transformed to 3D meshes, to represent 3D object shapes. The shape codes  $c$  is derived from the MLPs,

$$c = \omega(E_G(G^\ddagger)). \quad (4)$$

Conditioned on the codes  $c$ , the latent diffusion model is trained to output latent  $s_0$  for 3D shape generation. More specifically, the diffusion model includes a forward diffusion process and a reverse diffusion process. The forward diffusion gradually adds random noise to the target latent  $s_0$  using a sequence of increasing noise schedules  $\beta_t \in \{\beta_1, \dots, \beta_{T-1}, \beta_T\}$ . The shape latent  $s_0$  is generated from the GT SDFs by the pre-trained and frozen VQ-VAE [54] encoder during the training phase. Assuming that

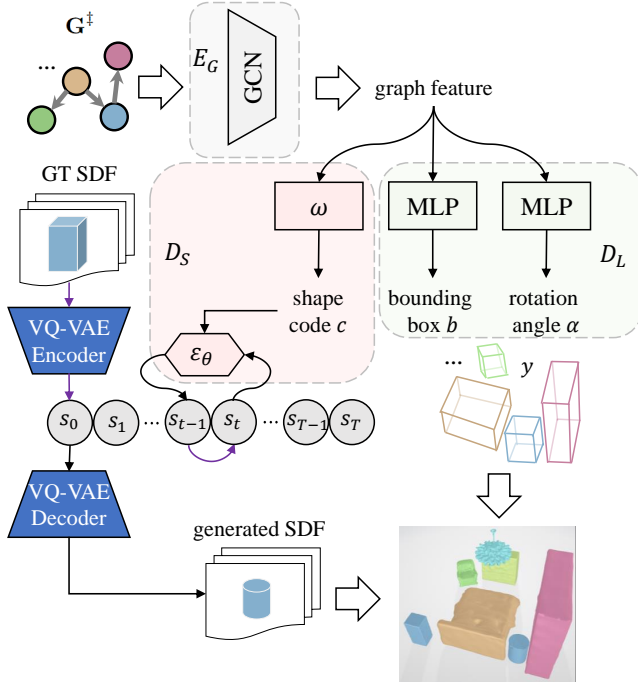


Fig. 4.  $E_G$  extracts shared graph features for the dual-branch decoder.  $D_L$  predicts 6-parameters 3D bounding boxes and their rotation angles. For  $D_S$ , the latent diffusion model with the denoiser  $\epsilon_\theta$  is conditioned on the shape code  $c$ , and the pre-trained and frozen VQ-VAE is applied to encode GT SDFs into the target latent  $s_0$  during training and decode the predicted latent back SDFs during inference.

$\delta_t := 1 - \beta_t$  and  $\bar{\delta}_t := \prod_{\kappa=1}^t \delta_\kappa$ , the noisy latent  $s_t$  is formulated as,

$$s_t = \sqrt{\bar{\delta}_t} s_0 + \sqrt{1 - \bar{\delta}_t} \epsilon, \quad (5)$$

where  $\epsilon$  is a Gaussian noise sampled from  $N(0, \mathcal{I})$ , and the time step  $t$  is sampled using the maximum time steps  $T$ . Starting from  $s_T \sim N(0, \mathcal{I})$ , the reverse diffusion denoises the noisy latent  $s_t$  back the target latent  $s_0$ . To this end, a trainable 3D-UNet [55] is regarded as a denoiser  $\epsilon_\theta$  which learns to predict the noise for the reverse diffusion process [4]. Besides, the pre-trained and frozen VQ-VAE decoder is applied to decode the predicted latent back SDFs during the inference phase.

### 3.3 Training Objectives

The proposed method is trained in an end-to-end manner.

For scene graph prior enhancement, the training objective is to minimize the Kullback-Liebler (KL) divergence between the posterior distribution  $p_\phi(z|x)$  and the distribution  $Z$ . The KL-based loss is formulated as,

$$\mathcal{L}_{KL} = D_{KL}(p_\phi(z|x) \| p(Z)). \quad (6)$$

For dual-branch graph-to-scene generation, the layout branch and shape branch are trained via layout loss  $\mathcal{L}_{layout}$  and shape loss  $\mathcal{L}_{shape}$ .

On one hand, we employ a commonly-used layout reconstruction loss,

$$\mathcal{L}_{rec}(\hat{y}, y) = \frac{1}{N} \sum_{i=1}^N (|\hat{b}_i - b_i| - \sum_{j=1}^{\Lambda} \hat{\alpha}_i^j \log \alpha_i^j), \quad (7)$$

where  $\hat{y} = \{\hat{b} \circ \hat{\alpha}\}$  are the GT layouts. The first term is the 3D bounding box regression loss, and the second is the rotation classification loss. The rotation space is divided into  $\Lambda$  bins. However, it is observed that the layout branch trained exclusively with reconstruction loss tends to handle simple scenes but suffers from unrealistic spatial arrangements for complex scenes. To improve the fidelity of generated layouts, we introduce an Intersection-over-Union (IoU) based regularization loss, defined as follows,

$$\mathcal{L}_{iou}(\hat{y}, y) = \sum_{i=1}^N (1 - IoU(\hat{y}_i, y_i)). \quad (8)$$

The regularization loss prevents layout collisions by encouraging the similarity between the predicted layouts and the corresponding GT layouts. Thus, the training objective of the layout branch is,

$$\mathcal{L}_{layout} = \mathcal{L}_{rec} + \eta \mathcal{L}_{iou}, \quad (9)$$

where  $\eta$  is used to balance these two loss items.

On the other hand, the shape branch is optimized through training the denoiser  $\epsilon_\theta$  with,

$$\mathcal{L}_{shape} = \|\epsilon - \epsilon_\theta(s_t, t, c)\|^2, \quad (10)$$

where  $t$  is sampled from discrete values  $\{1, \dots, T-1, T\}$ .

The overall training loss function comprises,

$$\mathcal{L} = \lambda_{KL} \mathcal{L}_{KL} + \lambda_{layout} \mathcal{L}_{layout} + \lambda_{shape} \mathcal{L}_{shape}, \quad (11)$$

where  $\lambda_{KL}$ ,  $\lambda_{layout}$  and  $\lambda_{shape}$  are weighting factors.

### 3.4 Inference

During the inference phase, the trained model  $\phi$  is used to estimate the distribution  $Z$ . Given a scene graph with initial object and relationship vectors  $\mathcal{V}_O$  and  $\mathcal{V}_R$ , the random vectors  $\mathcal{V}_O^Z$  are sampled from the estimated distribution  $Z$  for graph nodes  $O$ . Meanwhile, the pre-trained CLIP text encoder is adopted to generate  $\mathcal{V}_O^C$  and  $\mathcal{V}_R^C$  for graph nodes  $O$  and edges  $R$ . With aggregated relationship triplets, the pre-trained LLM is utilized to generate a sentence embedding  $\mathcal{V}^F$ . These vectors are incorporated as shown in Equation (2), resulting in the graph representation  $\mathbf{G}^\ddagger$ .

Next, the trained graph encoder  $E_G$  infers graph features from the graph representation  $\mathbf{G}^\ddagger$ . The object layouts  $y$  and the shape codes  $c$  are predicted via Equations (3) & (4). The latent  $s'_0$  is derived using the trained  $c$ -conditioned denoiser  $\epsilon_\theta$  by,

$$s'_0 = \frac{1}{\sqrt{\bar{\delta}_t}} (s_t - \sqrt{1 - \bar{\delta}_t} \epsilon_\theta(s_t, t, c)), \quad (12)$$

and it is then leveraged to reconstruct SDFs with the pre-trained VQ-VAE decoder. Finally, 3D scenes can be synthesized by fitting the 3D object shapes to the generated layouts.

## 4 EXPERIMENTS

In this section, we clarify the experimental settings, including dataset, evaluation metrics and implementation details. Then, the quantitative and qualitative results are shown and analyzed based on comparisons. Ablations studies are conducted to further verify the effects of the proposed components. Besides, we provide a user study.

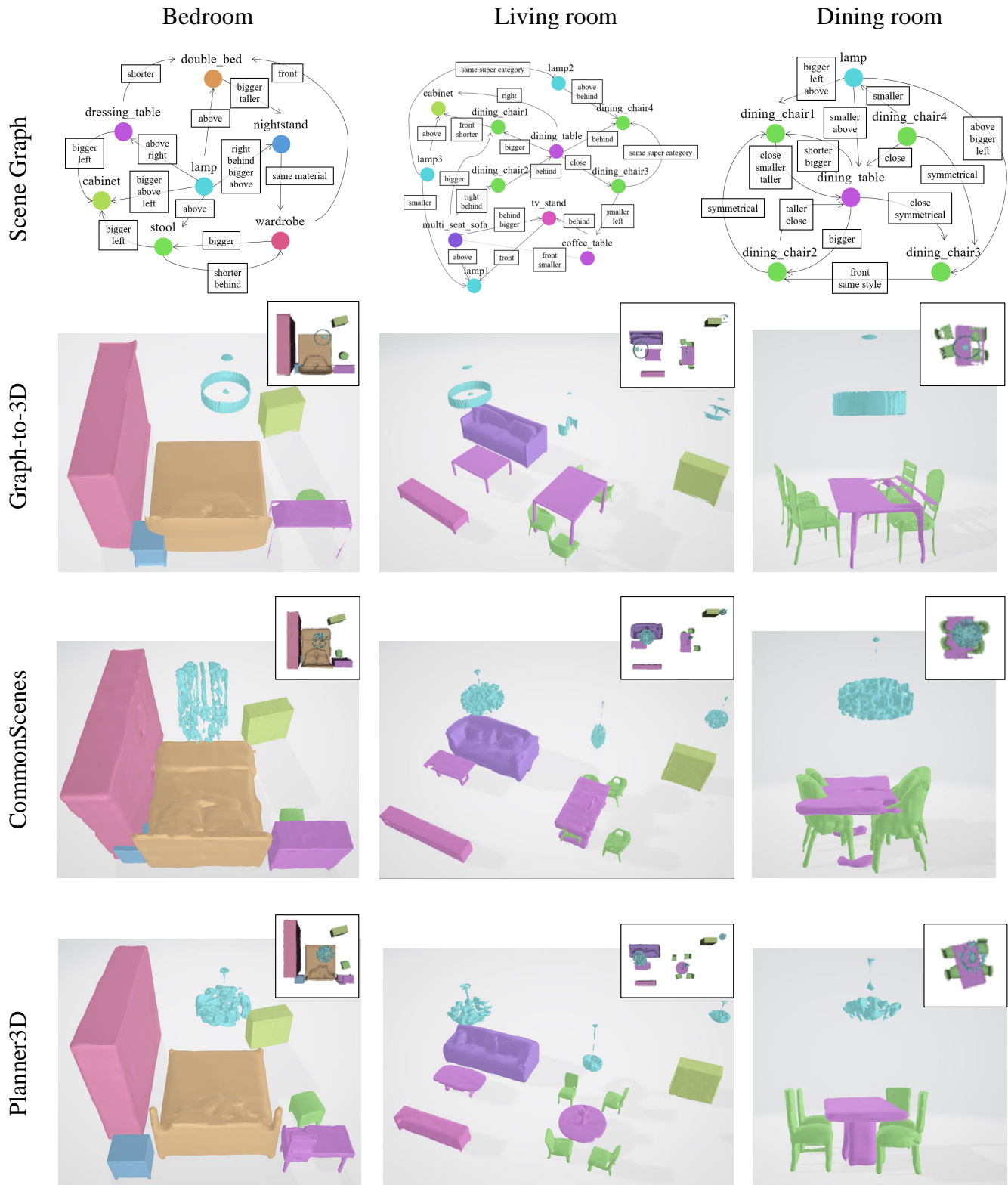


Fig. 5. Qualitative examples of bedroom, living room and dining room. Compared to Graph-to-3D [19] and CommonScenes [20], Planner3D shows higher fidelity with less interpenetrating phenomena.

## 4.1 Dataset

Our method is validated on SG-FRONT [20], a recent benchmark dataset providing scene graph annotations for 3D-FRONT dataset [56] which populates 3D scenes using furniture objects from 3D-FUTURE dataset [35]. SG-FRONT covers three room types of indoor scenes: 4,041 bedrooms, 900 dining rooms, and 813 living rooms. Following the original splits [20], 3,879 bedrooms, 614 dining rooms, and 544 living rooms are used for training, and the remaining ones are used for testing. Each room typically contains multiple objects, ending up with 45K object samples in total. The scene compositions are described by scene graphs, where nodes are defined by object categories and edges are mainly spatial relationships (e.g., *left/right of*, *close by*) between objects. Overall, SG-FRONT dataset has 35 object categories and 15 relationship categories.

## 4.2 Evaluation Metrics

The synthesized 3D scenes are evaluated from three aspects:

**Scene graph consistency.** Using pre-defined geometric constraints, the scene graph consistency is measured to assess the spatial consistency between the generated layouts and the corresponding relationships specified in the given graph edges. Specifically, we validate "easy" relationships including *left/right*, *front/behind*, *bigger/smaller than*, *taller/shorter than*, as well as "hard" relationships including *close by* and *symmetrical to*. These relationships correspond to the geometric rules depicted in Table 1.  $IoU(\cdot)$ ,  $Cor(\cdot)$ ,  $Dis(\cdot)$  and  $Fli(\cdot)$  denote the processes of calculating IoUs, bounding box corners, distances, and flipping based on  $x$ -axis or  $y$ -axis, respectively. The bounding box  $b_i$  is composed of the bottom center coordinates  $\{x_i, y_i, z_i\}$ , width  $w_i$ , length  $l_i$  and height  $h_i$ . For fair comparisons, we employ the thresholds used in previous works.

**Object-level fidelity.** The shape fidelity is reported by Chamfer Distance (CD) [59] based Minimum Matching Distance (MMD), Coverage (COV), and 1-Nearest Neighbor Accuracy (1-NNA) [60], which are computed via Equations (13), (14), (15) and (16).

$$CD(P, \hat{P}) = \sum_{p \in P} \min_{\hat{p} \in \hat{P}} \|p - \hat{p}\|_2^2 + \sum_{\hat{p} \in \hat{P}} \min_{p \in P} \|p - \hat{p}\|_2^2, \quad (13)$$

where  $P$  and  $\hat{P}$  are point clouds sampled from the generated shape and the corresponding GT shape, respectively.

$$MMD(X, \hat{X}) = \frac{1}{|\hat{X}|} \sum_{\hat{P} \in \hat{X}} \min_{P \in X} CD(P, \hat{P}), \quad (14)$$

$$COV(X, \hat{X}) = \frac{|\{\text{argmin}_{\hat{P} \in \hat{X}} CD(P, \hat{P}) | P \in X\}|}{|\hat{X}|}, \quad (15)$$

$$1 - NNA(X, \hat{X}) = \frac{\sum_{P \in X} \mathbb{I}[N_P \in X] + \sum_{\hat{P} \in \hat{X}} \mathbb{I}[N_{\hat{P}} \in \hat{X}]}{|X| + |\hat{X}|}, \quad (16)$$

where  $X$  and  $\hat{X}$  are the generated scene collection and the GT scene collection, respectively. In addition,  $\mathbb{I}[\cdot]$  is the indicator function, and  $N_P$  is the CD-based nearest neighbor of  $P$  in  $X_{-P} = \hat{X} \cup X - \{P\}$ .

**Scene-level fidelity.** To evaluate the quality of scene synthesis from a global perspective, we report two metrics: FID [57] and KID [58], which are calculated with the top-down renderings of the synthesized and reference 3D scenes. Following prior works, scene-level fidelity acts as the most important evaluation metric.

TABLE 1  
Definitions of geometric constraints between two instances  $i$  and  $j$ .

Relationship	Rule
<i>left of</i>	$x_i < x_j$ and $IoU(b_i, b_j) < 0.3$
<i>right of</i>	$x_i > x_j$ and $IoU(b_i, b_j) < 0.3$
<i>front of</i>	$y_i < y_j$ and $IoU(b_i, b_j) < 0.3$
<i>behind of</i>	$y_i > y_j$ and $IoU(b_i, b_j) < 0.3$
<i>bigger than</i>	$(w_i l_i h_i - w_j l_j h_j) / w_i l_i h_i > 0.15$
<i>smaller than</i>	$(w_i l_i h_i - w_j l_j h_j) / w_i l_i h_i < -0.15$
<i>taller than</i>	$((z_i + h_i) - (z_j + h_j)) / (z_i + h_i) > 0.1$
<i>shorter than</i>	$((z_i + h_i) - (z_j + h_j)) / (z_i + h_i) < -0.1$
<i>close by</i>	$Dis(Cor(b_i), Cor(b_j)) < 0.45$
<i>symmetrical to</i>	$Dis(Fli(b_i), b_j) < 0.45$

## 4.3 Implementation Details

Regarding scene graph prior enhancement, we set the feature dimension  $Q$  as 64. The CLIP-based vectors are 512-dimensional, i.e.,  $\mathcal{V}_O^C \in \mathbb{R}^{N \times 512}$  and  $\mathcal{V}_R^C \in \mathbb{R}^{M \times 512}$ . Since Instructor Transformer can generate text embedding tailored to diverse domains (e.g., medicine, finance, and science) and tasks (e.g., retrieval, and summarization), we exploit the instruction "Represent the Science document for summarization" to specify the LLM usage goal. The dimension of the LLM-based vector  $\mathcal{V}^F$  is 768. Five GCN layers are exploited to extract graph  $\mathbf{G}^\dagger$  features, which are then feed with two MLP modules. The dimension of  $\mu_b$  and  $\sigma_b$  is 48, and the dimension of  $\mu_\alpha$  and  $\sigma_\alpha$  is 16. After the concatenation process, the resulting  $\mu$  and  $\sigma$  are 64-dimensional and the distribution  $Z \sim \mathcal{N}(\mu, \sigma)$  is 64-dimensional Gaussian distribution. The layout feature vectors  $\mathcal{V}_O^B$  are only used for training and not needed for inference phase, hence, the inference starts from constructing the scene graph representation  $\mathbf{G}^\ddagger$ . Regarding dual-branch graph-to-scene generation, the graph encoder  $E_G$  employs 5 GCN layers. With shared graph features, the model  $\omega$ , consisting of 3 stacked MLP layers, predicts the shape code  $c$  which is a 1280-dimensional vector and conditions the denoiser  $\epsilon_\theta$ . The resolution of SDF is 64, i.e.  $SDF \in \mathbb{R}^{64 \times 64 \times 64}$ . The shape latent  $s_0 \in \mathbb{R}^{16 \times 16 \times 16}$ . For the latent diffusion model, the time step  $T$  is set to 1000. The layout decoder  $D_L$  takes graph features as inputs and utilize two groups of 3 stacked MLPs to estimate 6-parameterized bounding box  $b$  and rotation angle  $\alpha$ . The whole framework is trained in an end-to-end manner with the AdamW optimizer [61] and the initial learning rate is set to  $1e^{-4}$ . The weighting factors  $\lambda_{KL}$ ,  $\lambda_{layout}$ ,  $\lambda_{shape}$  are set to 1.0, while  $\eta$  is set to 0.01. For the rotation classification,  $\Lambda$  is set to 24. The batch size is 32. All the experiments are conducted on a single NVIDIA A40 GPU with 46GB memory.

TABLE 2

Comparisons with Graph-to-3D [19] and CommonScenes [20] on scene graph consistency (higher is better). The best results are shown in **bold**.

Method	Easy				Hard		mSG
	<i>left/right</i> ↑	<i>front/behind</i> ↑	<i>big/small</i> ↑	<i>tall/short</i> ↑	<i>close</i> ↑	<i>symmetrical</i> ↑	
Graph-to-3D [19] (*)	<b>0.98</b>	0.99	0.96	0.93	0.74	0.50	0.87
CommonScenes [20] (*)	<b>0.98</b>	<b>1.00</b>	<b>0.97</b>	<b>0.96</b>	<b>0.76</b>	<b>0.62</b>	<b>0.90</b>
Graph-to-3D [19]	<b>0.98</b>	0.99	<b>0.97</b>	0.96	0.75	0.64	<b>0.90</b>
CommonScenes [20]	<b>0.98</b>	0.99	<b>0.97</b>	0.96	0.76	<b>0.66</b>	<b>0.90</b>
Planner3D	<b>0.98</b>	<b>1.00</b>	<b>0.97</b>	<b>0.97</b>	<b>0.77</b>	<b>0.66</b>	<b>0.90</b>

TABLE 3

Comparisons with Graph-to-3D [19] and CommonScenes [20] on object-level fidelity. MMD ( $\times 0.01$ ), COV (%) and 1-NNA (%) are computed. Total is calculated as the mean values across categories. The best results are shown in **bold**.

Category	MMD↓			COV↑			1-NNA↓		
	[19]	[20]	Ours	[19]	[20]	Ours	[19]	[20]	Ours
Bed	<b>1.27</b>	1.47	1.73	<b>10.34</b>	5.17	4.31	97.41	<b>92.62</b>	93.44
Nightstand	<b>3.00</b>	7.12	4.49	<b>11.21</b>	6.03	6.03	98.28	<b>93.60</b>	<b>93.60</b>
Wardrobe	<b>1.15</b>	3.11	1.41	<b>7.76</b>	2.59	6.03	97.41	97.56	<b>91.87</b>
Chair	<b>2.28</b>	2.57	3.10	8.62	<b>9.48</b>	6.90	97.41	<b>93.23</b>	<b>93.23</b>
Table	5.68	4.98	<b>4.27</b>	8.62	<b>12.07</b>	10.34	96.98	<b>86.57</b>	88.06
Cabinet	2.57	3.45	<b>2.41</b>	5.17	5.17	<b>9.48</b>	96.45	96.21	<b>88.64</b>
Lamp	4.00	2.78	<b>2.44</b>	7.76	10.34	<b>12.07</b>	98.71	86.86	<b>81.75</b>
Shelf	6.60	5.43	<b>3.14</b>	6.67	20.00	<b>26.67</b>	96.00	<b>56.52</b>	65.22
Sofa	1.31	1.11	<b>1.08</b>	0.86	6.90	<b>9.48</b>	99.04	<b>93.75</b>	96.88
TV stand	0.98	<b>0.62</b>	0.84	2.59	<b>12.93</b>	6.03	98.02	<b>90.91</b>	94.70
Total	2.88	3.26	<b>2.49</b>	6.96	9.07	<b>9.73</b>	97.57	88.78	<b>88.74</b>

TABLE 4

Comparisons with Graph-to-3D [19] and CommonScenes [20] on scene-level fidelity in SG-FRONT dataset [20] (lower is better). FID and KID ( $\times 0.001$ ) are computed based on the top-down images (256 $\times$ 256 pixels) rendered from the synthesized and reference 3D scenes. (\*) denotes the shape retrieval version of the method where only layout branch is utilized. The best results are shown in **bold**.

Method	Bedroom		Living room		Dining room		All	
	FID↓	KID↓	FID↓	KID↓	FID↓	KID↓	FID↓	KID↓
Graph-to-3D [19] (*)	<b>60.48</b>	<b>7.85</b>	81.31	3.97	67.40	5.88	<b>45.89</b>	<b>4.34</b>
CommonScenes [20] (*)	64.91	13.23	<b>78.24</b>	<b>2.65</b>	<b>65.48</b>	<b>4.13</b>	47.22	5.98
Graph-to-3D [19]	68.37	17.97	92.50	18.48	71.13	7.76	51.91	9.25
CommonScenes [20]	65.26	12.79	85.87	8.89	69.67	6.71	49.89	7.37
Planner3D	<b>60.47</b>	<b>9.30</b>	<b>82.99</b>	<b>8.51</b>	<b>69.40</b>	<b>6.39</b>	<b>47.34</b>	<b>6.13</b>

#### 4.4 Quantitative Results and Comparisons

The proposed Planner3D is compared with two recent state-of-the-art scene graph-to-3D scene synthesis methods: Graph-to-3D [19] and CommonScenes [20]<sup>1</sup>.

First, we report the performance in terms of scene graph consistency, as shown in Table 2 where mSG indicates the mean scene graph consistency computed on both easy and hard relationships. In general, with joint layout-shape learning frameworks, (semi-) generative methods derive better consistency than retrieval-based methods (\*) that only learn layout synthesis. These methods yield close mSG values due to their comparable performance on easy relationships. Still, Planner3D achieves the best results overall because it performs relatively superior to SOTAs on hard relationships.

Second, we provide object-level fidelity comparisons of shape generative methods. Table 3 shows the results of 10 object categories on MMD, COV and 1-NNA. In terms of MMD score (lower is better), Planner3D is 0.39 lower than Graph-to-3D [19] and 0.77 lower than CommonScenes [20]. In terms of COV score (higher is better), Planner3D is 2.77 higher than Graph-to-3D [19] and 0.7 higher than

CommonScenes [20]. In terms of 1-NNA score (lower is better), Planner3D is 8.83 lower than Graph-to-3D [19] and 0.04 lower than CommonScenes [20]. Overall, our method attains better results compared to Graph-to-3D [19] and CommonScenes [20], which suggests the object-level shape generation ability of the proposed method.

Lastly, we report the results on scene-level fidelity, as shown in Table 4. The top two rows are shape retrieval-based methods (i.e., only layout branch is trained and tested) and the bottom three are joint shape and layout learning-based methods. Since 3D shapes are directly retrieved from the database, the retrieval-based methods (\*) usually achieve lower FIDs and KIDs than (semi-) generative methods. However, shape retrieval-based methods are heavily bounded by the scale and reliability of the given databases. For all the room types, our method has 47.34 FID score and 6.13 KID score. Compared to the Graph-to-3D [19], our method has reached 4.57 lower FID score, 3.12 lower KID score. Compared to the state-of-the-art CommonScenes [20], our method has reached 2.55 lower FID score, 1.24 lower KID score. Overall, Planner3D obtains the best FID and KID scores on all the room types (lower score indicates better performance). Surprisingly, the proposed method even achieves the best performance with retrieval-based

1. All the results of Graph-to-3D [19] and CommonScenes [20] presented in this paper are reproduced using the official code with default settings.

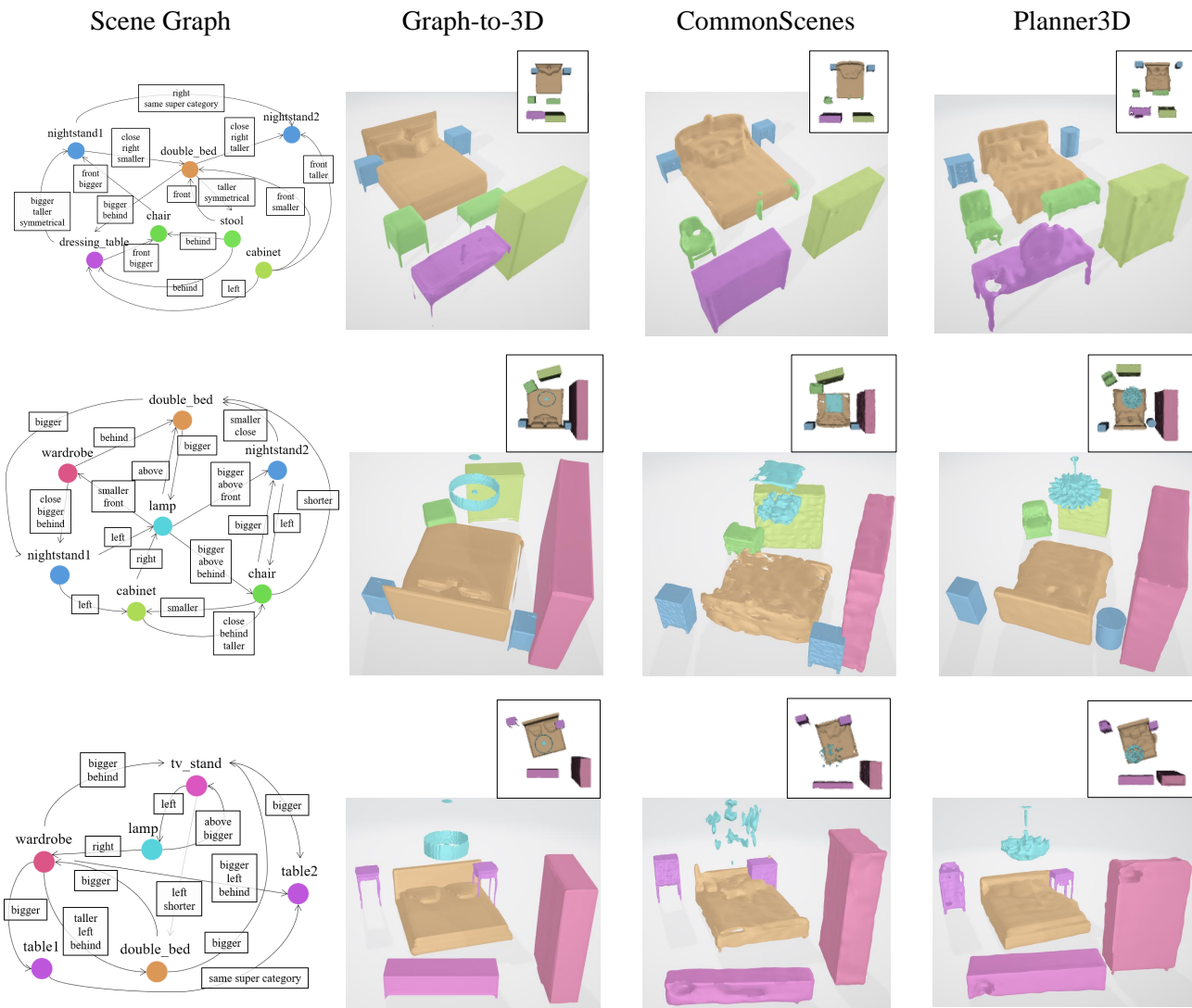


Fig. 6. Additional qualitative comparisons on bedroom scenes. A side view of each 3D scene is provided with a top-down view.

TABLE 5  
Scene-level fidelity comparisons on all room types by running the evaluations 5 times. The best results are shown in **bold**.

Method	FID↓	KID↓
Graph-to-3D [19]	51.916±0.002	9.250±0.004
CommonScenes [20]	49.859±0.303	7.533±0.262
Planner3D	<b>47.486±0.278</b>	<b>6.254±0.394</b>

methods on the FID score in Bedroom scenes. Furthermore, Table 5 reports the FID and KID values on **all** the room types by running the evaluations 5 times, demonstrating the effectiveness and stability of Planner3D.

#### 4.5 Qualitative Results and Comparisons

Given the scene graph inputs, qualitative results on bedroom, living room and dining room are shown in Fig. 5. Overall, Graph-to-3D [19] and CommonScenes [20] tend to synthesize unrealistic 3D scenes in which ambiguous shapes (e.g., broken dining table) and interpenetrating phenomena (e.g., table and chair intersect with each other) commonly happen. In contrast, Planner3D is able to generate much

more realistic 3D scenes with reasonable spatial arrangements and shape generation.

On one hand, our layout synthesis is constrained with IoU-based regularization, which efficiently alleviates object collision problems compared to those un-regularized layout regression approaches, as shown in the nightstand-double bed-wardrobe case of Fig. 5 bedroom. On the other hand, we notice that the 3D shapes generated from Planner3D are more controllable and not as random as prior works. It can be seen from the table-and-chair cases in Fig. 5, the table is generated as round shape (in living room) or with single table leg (in dining room), which match the arrangements of the surrounding chairs. Without special designs, our shape branch benefits from the proposed scene graph prior enhancement mechanism, and the shared graph feature encoding with the layout branch which enables joint layout-shape learning at an early stage.

More visualizations of the bedroom, living room and dining room results are provided in Figs. 6, 7, and 8, respectively. It can be seen that Graph-to-3D [19] usually generates

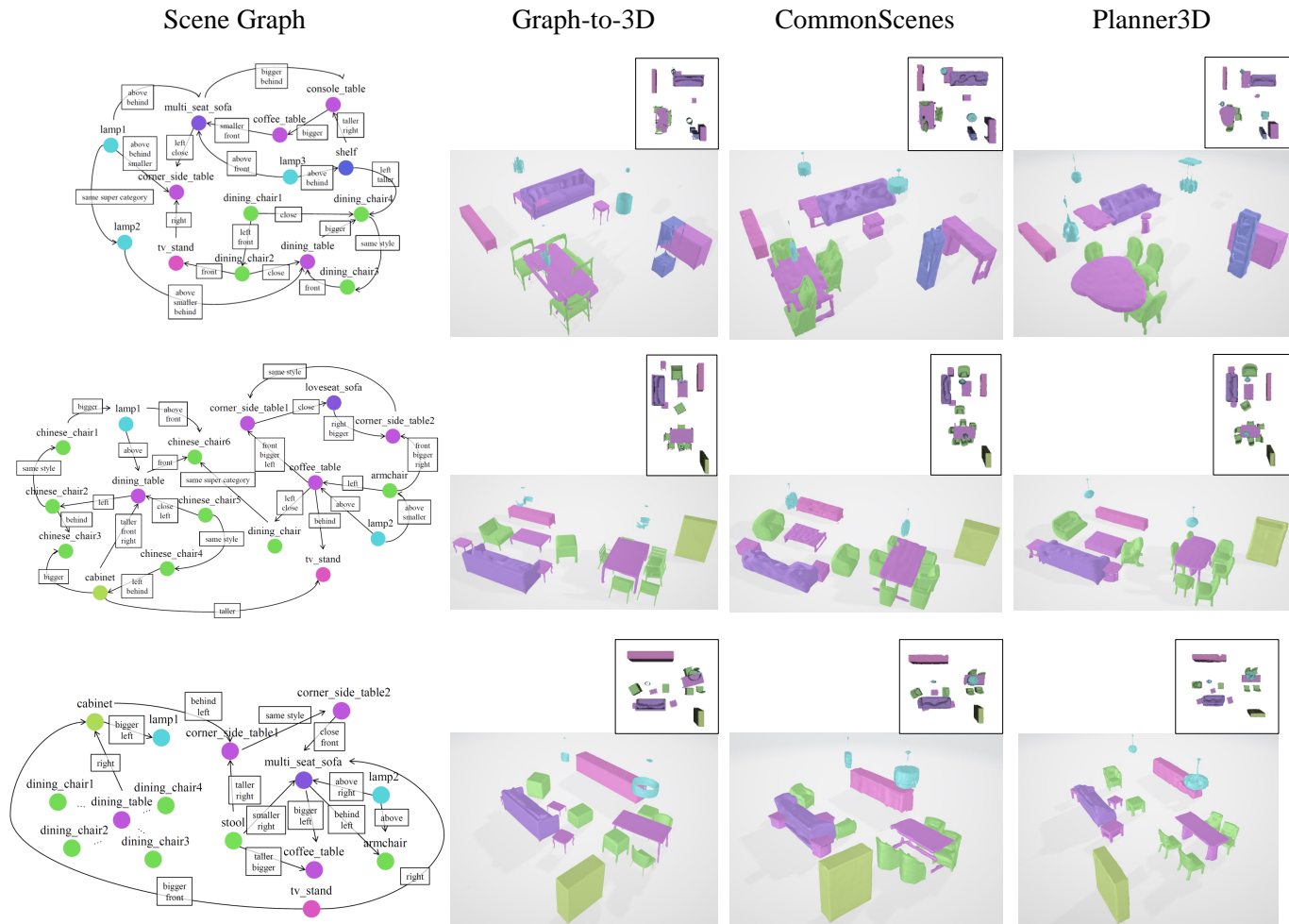


Fig. 7. Additional qualitative comparisons on living room scenes. A side view of each 3D scene is provided with a top-down view.

TABLE 6  
Ablation study results on all room types of SG-FRONT dataset. The best results are shown in **bold**.

Method	Scene-level fidelity		Scene graph consistency						
	FID↓	KID↓	mSG↑	left/right↑	front/behind↑	big/small↑	tall/short↑	close↑	symmetrical↑
Planner3D (Ours)	<b>47.34</b>	<b>6.13</b>	<b>0.90</b>	<b>0.98</b>	<b>1.00</b>	<b>0.97</b>	<b>0.97</b>	<b>0.77</b>	<b>0.66</b>
w/o LLM	47.71	7.94	0.88	<b>0.98</b>	0.99	0.96	0.95	<b>0.77</b>	0.54
w/o Reg	48.15	6.93	<b>0.90</b>	<b>0.98</b>	0.99	<b>0.97</b>	<b>0.97</b>	0.76	0.62

3D scenes composed of regular object shapes and performs well for simple scenes such as bedrooms. However, the quality of generated objects degrades as the number of objects increases, e.g., on living rooms and dining rooms. Note that due to limited space, we partially visualize the scene graphs, e.g., the last scene graph of Fig. 7. Besides, it is observed that Graph-to-3D suffers from limited shape diversity. For instance, it generates a specific 3D shape for the object *lamp* across different scenes. Benefiting from the diffusion-based shape branch, CommonScenes [20] is able to synthesize diverse and plausible 3D object shapes, but the generated scenes are often unrealistic due to low-quality shapes and object collisions. In contrast, Planner3D performs better at object-level and scene-level. It is worth pointing out that the 3D scenes generated by Planner3D exhibit more realistic shapes and reasonable layout configurations.

TABLE 7  
Ablation study results w.r.t. layout discriminator and unified graph encoder. The mSG values are computed on both easy and hard relationships. The best results are shown in **bold**.

Method	FID↓	KID↓	mSG↑
CommonScenes [20]	49.89	7.37	0.90
w/o Dis	48.20	6.73	0.88
w Uni	47.69	6.54	0.89
Planner3D (Ours)	<b>47.34</b>	<b>6.13</b>	0.90
w Dis	49.09	8.74	<b>0.91</b>

## 4.6 Ablation Study

Firstly, we assess the effects of the proposed key components in Planner3D: LLM-based scene graph prior enhancement (abbreviated as *LLM*) and explicit layout regularization (abbreviated as *Reg*). Using the metrics in terms of

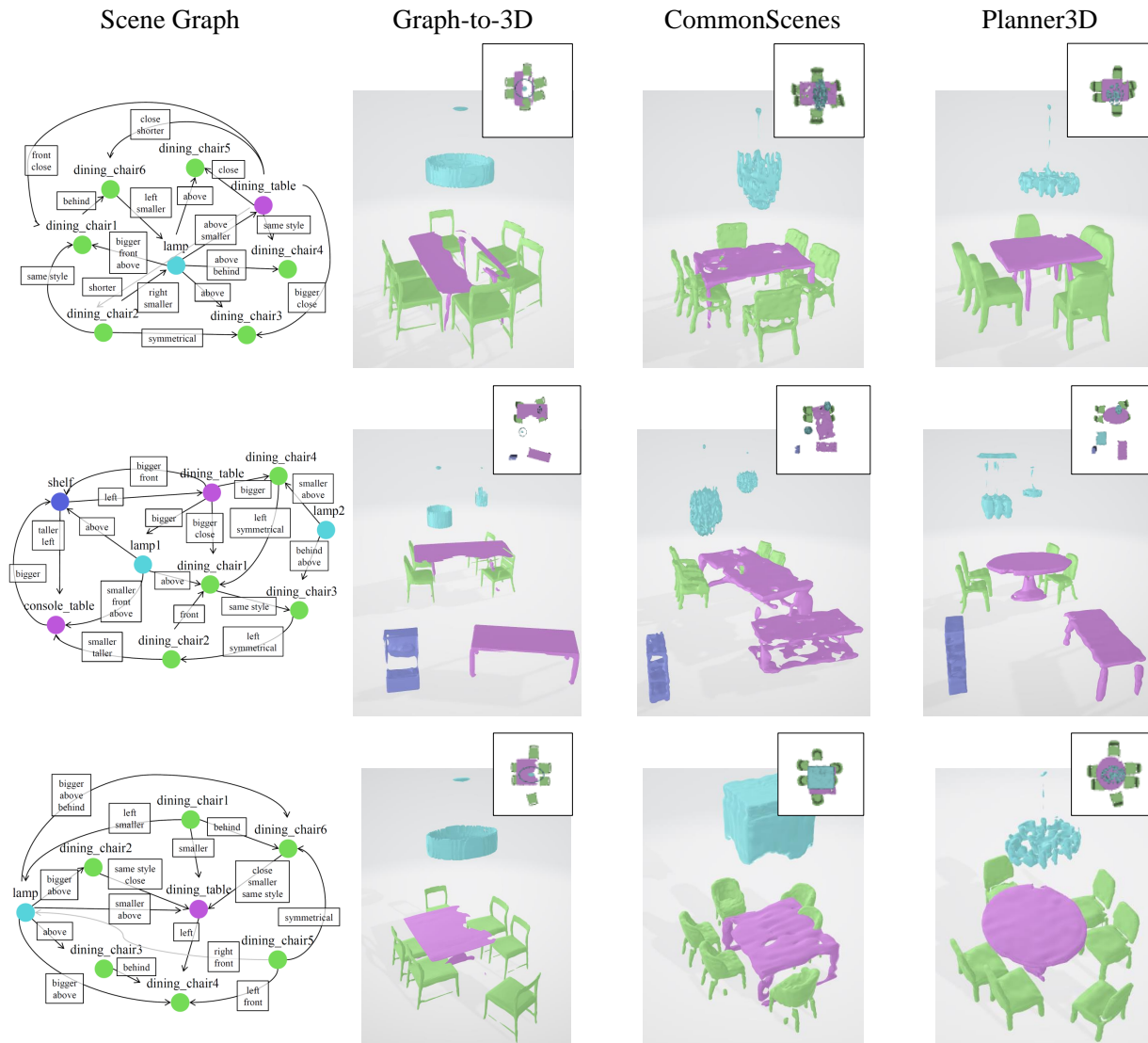


Fig. 8. Additional qualitative comparisons on dining room scenes. A side view of each 3D scene is provided with a top-down view.

scene-level fidelity and scene graph consistency, the results are shown in Table 6. The first row illustrates our full model, i.e., Planner3D. In contrast, *LLM* supports FID and mSG, and introduces significant improvement on KID and the hard relationship *symmetrical*. This demonstrates the advantage of LLM-based scene graph prior enhancement, which provides rich signals for the following encoding stage. As shown in the last row, *Reg* contributes scene-level fidelity, especially on FID. By jointly applying layout regression and explicit regularization, the spatial arrangements of objects become more realistic with fewer collision issues. Fig. 9 demonstrates two living room examples which are synthesized without and with *Reg*, respectively. It can be seen from the left column that the scene quality drops significantly due to the overlapping objects. Instead, explicit regularization facilitates reasonable spatial arrangement, as shown in the right column.

Secondly, we investigate the performance of the discriminator (abbreviated as *Dis*) that is commonly used for layout synthesis in prior works [19], [20], as well as the

proposed unified graph encoder (abbreviated as *Uni*). The results are listed in Table 7. Taking the results of the baseline CommonScenes [20] as an example, the FID, KID and mSG values all decrease without *Dis*, which indicates that adversarial training is not an optimal solution to layout synthesis. As can be seen from the bottom two rows, *Dis* offers only slight improvements to scene graph consistency while compromising scene-level fidelity. This proves the claim that GAN-based layout synthesis suffers from training instability and affects the training quality of layout decoder. Rather than training with *Dis*, Planner3D is more robust by explicit layout regularization, achieving better trade-off between scene-level fidelity and scene graph consistency. In addition, even with less learnable parameters, CommonScenes with the unified graph encoder outperforms the raw CommonScenes which utilizes separate graph encoders. The unified graph encoder, which acts as a bridge between LLM-enhanced scene graph prior and dual-branch scene decoder, enables effective integration of layout branch and shape branch under the guidance of shared graph features.

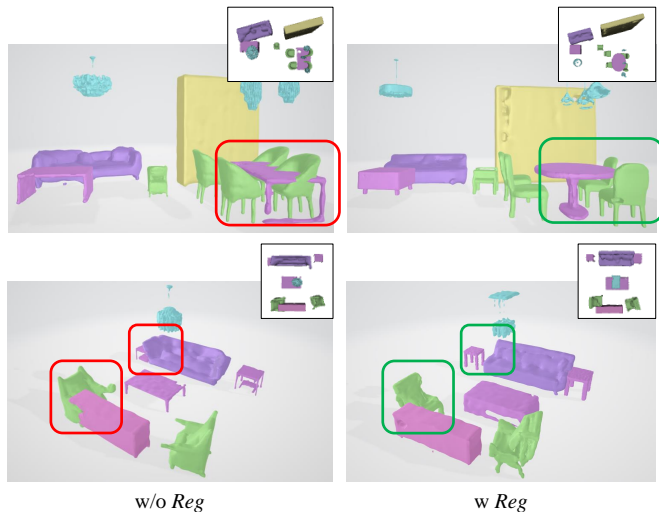


Fig. 9. Without *Reg*, unrealistic layouts (highlighted in red rectangles) frequently appear. In contrast, applying *Reg* typically results in well-structured layouts, highlighted in green rectangles. A side view of each 3D scene is provided with a top-down view.

#### 4.7 User Study

Although the evaluation metrics can indicate the quality of the generated 3D scenes, they cannot be fully equated with human perception. Therefore, we invited  $\sim 30$  participants from various professional backgrounds to perform a user study. Fig. 10 shows the user interface of this study.

Overall, we randomly sampled 15 scenes covering all room types, and the synthesized 3D scenes were the results of Graph-to-3D [19], CommonScenes [20] and our Planner3D, respectively. To ensure the visibility, the scenes were rendered from a side view and a top-down view. Due to space limitation, only parts of relationships (i.e., edges) are shown in the scene graphs. Given the paired scene graph input and the 3D scenes synthesized by different methods, participants were requested to vote for the best scene based on three criteria: scene-level realism (SR), object-level quality (OQ), and layout correctness (LC). They were described to the participants by:

**SR:** *Does the scene look realistic and stylistically coherent?*

**OQ:** *Do the objects have high-quality 3D shapes?*

**LC:** *Does the spatial arrangement of objects appear correct and free of collision?*

Basically, SR requires participants to check whether the scene is realistic and coherent, acting as a global indicator that considers both 3D shapes and layouts. OQ emphasizes the completeness and fidelity of the generated object shapes, while LC denotes the spatial arrangement levels of objects.

The average results are given in Table 8. Most of the participants (48.3%) suggested that our generated scenes were preferred over the other methods on the scene-level realism. Where Graph-to-3D was instead preferred 42.5% and CommonScenes was preferred 9.2%. Regarding the object-level quality, most of the participants (49.7%) preferred the results of Graph-to-3D, without being informed that the inflexibility of its shape generation which relies on pre-trained shape codes from category-wise auto-decoders. CommonScenes and Planner3D were preferred 10% and 40.3%, respectively. Furthermore, Planner3D was preferred

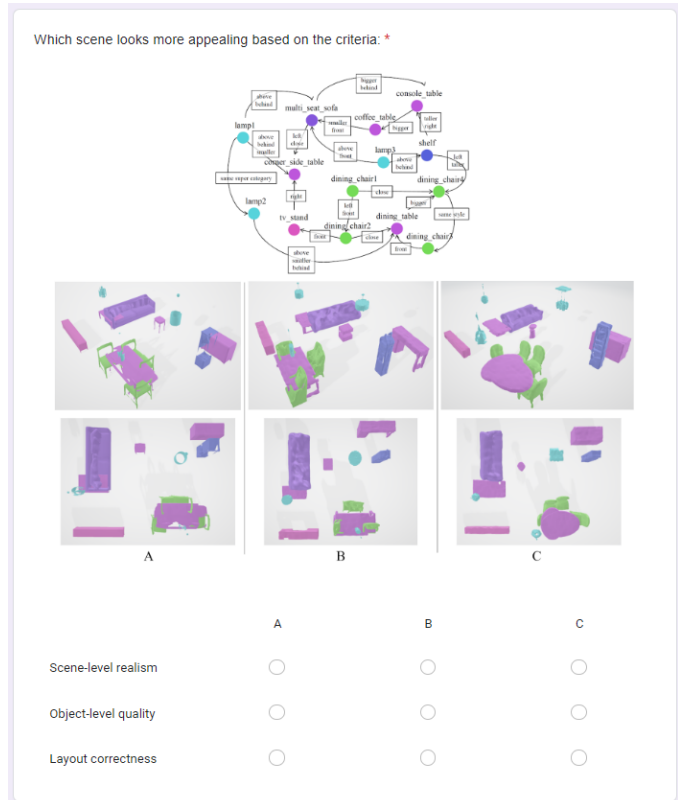


Fig. 10. User interface for the user study.

TABLE 8  
User study results via the percentage of voters.

Method	SR	OQ	LC
Graph-to-3D [19]	42.5%	49.7%	31.7%
CommonScenes [20]	9.2%	10.0%	7.8%
Planner3D	48.3%	40.3%	60.5%

60.5% on the layout correctness, much higher than other methods Graph-to-3D 31.7% and CommonScenes 7.8%, demonstrating its superiority on spatial arrangements of objects. Interestingly, our baseline method CommonScenes obtained the lowest voting rates on all the criteria of this study, even it outperformed Graph-to-3D on the evaluation metrics shown in the main paper. This perceptual user study shows that the proposed method improves compositional 3D scene synthesis compared to the baselines, and enjoys high flexibility without being dependent on per-category shape codes and adversarial training.

## 5 DISCUSSION

### 5.1 Broader Impact

We believe Planner3D will be applied to interior design, game development, augmented and virtual reality applications. By designing scene graphs, users can create realistic and coherent 3D indoor scenes tailored to their specifications, without the need for specialized 3D modeling expertise. For textured 3D indoor scenes, Planner3D can work with recent 3D scene texturing works, such as MVDiffusion [63] and SceneTex [62], through providing high-quality

semantic scenes. As large language models continue to advance rapidly, the integration of more powerful LLMs, e.g., GPT series [66], [67] and Llama [68], into our pipeline offers substantial potential for improving both the controllability and scalability of 3D scene synthesis.

## 5.2 Limitations

Despite the advancements, there are still some limitations of the proposed method. First of all, the scale of the 3D scene dataset we employed remains small. SG-FRONT [20] offers thousands of samples covering three room types, whereas 3D object datasets [36], [37] typically provide millions of or even more samples. Hence, expanding the existing scene dataset via leveraging large-scale 3D object datasets would be an interesting research direction. The scene graph annotations can be derived from natural language descriptions which are easily obtained. Planner3D is originally developed with a focus on indoor scene synthesis from scene graph. However, the presented pipeline shows potential for adapting to larger-scale outdoor scenes (e.g., [64], [65]), which is also a critical and promising topic. On one hand, the open-vocabulary nature and reasoning ability of LLMs could support our scene graph prior enhancement for handling with complex scene-object relationships. On the other hand, our explicit layout regularization can alleviate the limitations of prior works on object spatial arrangements. We will explore these ideas in future work.

## 6 CONCLUSIONS

In this work, we present Planner3D, a simple yet effective scene graph-to-3D scene synthesis method which outperforms previous state-of-the-art methods by a large margin. LLMs are integrated with CLIP to enhance the scene graph representations, enabling a hierarchical understanding of graph priors. A unified graph encoder extracts shared graph features that guide a dual-branch scene decoder. A latent diffusion model is trained at the shape branch. The layout branch is optimized with explicit regularization, instead of adopting adversarial training scheme that suffers from ambiguous spatial arrangements. Experimental results show the superiority of Planner3D in terms of scene graph consistency, object-level fidelity and scene-level fidelity.

## REFERENCES

- [1] Kingma, Diederik P and Welling, Max, *Auto-encoding variational bayes*. arXiv preprint arXiv:1312.6114, 2013. 1, 2
- [2] Goodfellow, Ian and Pouget-Abadie, Jean and Mirza, Mehdi and Xu, Bing and Warde-Farley, David and Ozair, Sherjil and Courville, Aaron and Bengio, Yoshua, *Generative adversarial nets*. Advances in neural information processing systems, 27, 2014. 1, 2
- [3] Rezende, Danilo and Mohamed, Shakir, *Variational inference with normalizing flows*, International conference on machine learning, 1530–1538, 2015. 1, 2
- [4] Ho, Jonathan and Jain, Ajay and Abbeel, Pieter, *Denoising diffusion probabilistic models*, Advances in neural information processing systems, 33, 6840–6851, 2020. 1, 2, 6
- [5] Ramesh, Aditya and Dhariwal, Prafulla and Nichol, Alex and Chu, Casey and Chen, Mark, *Hierarchical text-conditional image generation with clip latents*, arXiv preprint arXiv:2204.06125, 2022. 1, 2
- [6] Tang, Jiayang and Ren, Jiawei and Zhou, Hang and Liu, Ziwei and Zeng, Gang, *Dreamgaussian: Generative gaussian splatting for efficient 3d content creation*, arXiv preprint arXiv:2309.16653, 2023. 1, 2
- [7] Liu, Ruoshi and Wu, Rundi and Van Hoorick, Basile and Tokmakov, Pavel and Zakharov, Sergey and Vondrick, Carl, *Zero-1-to-3: Zero-shot one image to 3d object*, Proceedings of the IEEE/CVF International Conference on Computer Vision, 9298–9309, 2023. 1
- [8] Liu, Minghua and Xu, Chao and Jin, Haian and Chen, Linghao and Varma T, Mukund and Xu, Zexiang and Su, Hao, *One-2-3-45: Any single image to 3d mesh in 45 seconds without per-shape optimization*, Advances in Neural Information Processing Systems, 36, 2024. 1
- [9] Jun, Heewoo and Nichol, Alex, *Shap-e: Generating conditional 3d implicit functions*, arXiv preprint arXiv:2305.02463, 2023. 1, 2
- [10] Tian, Xi and Yang, Yong-Liang and Wu, Qi, *ShapeScaffolder: Structure-Aware 3D Shape Generation from Text*, Proceedings of the IEEE/CVF International Conference on Computer Vision, 2715–2724, 2023. 1, 2
- [11] Zhou, Linqi and Du, Yilun and Wu, Jiajun, *3D shape generation and completion through point-voxel diffusion*, Proceedings of the IEEE/CVF International Conference on Computer Vision, 5826–5835, 2021. 1, 2
- [12] Liu, Zhengzhe and Dai, Peng and Li, Ruihui and Qi, Xiaojuan and Fu, Chi-Wing, *Iss: Image as setting stone for text-guided 3d shape generation*, arXiv preprint arXiv:2209.04145, 2022. 1, 2
- [13] Wei, Yao and Vosselman, George and Yang, Michael Ying, *Flow-based GAN for 3D point cloud generation from a single image*, British Machine Vision Conference, 2022. 1, 2
- [14] Cheng, Yen-Chi and Lee, Hsin-Ying and Tulyakov, Sergey and Schwing, Alexander G and Gui, Liang-Yan, *Sdfusion: Multimodal 3d shape completion, reconstruction, and generation*, Proceedings of the IEEE/CVF Conference on Computer Vision and Pattern Recognition, 4456–4465, 2023. 1, 2
- [15] Ren, Xuanchi and Huang, Jiahui and Zeng, Xiaohui and Museth, Ken and Fidler, Sanja and Williams, Francis, *XCube: Large-Scale 3D Generative Modeling using Sparse Voxel Hierarchies*, arXiv preprint arXiv:2312.03806, 2023. 1, 3
- [16] Engelmann, Francis and Rematas, Konstantinos and Leibe, Bastian and Ferrari, Vittorio, *From points to multi-object 3D reconstruction*, Proceedings of the IEEE/CVF conference on computer vision and pattern recognition, 4588–4597, 2021. 1, 3
- [17] Po, Ryan and Wetzstein, Gordon, *Compositional 3d scene generation using locally conditioned diffusion*, arXiv preprint arXiv:2303.12218, 2023. 1, 3
- [18] Luo, Andrew and Zhang, Zhoutong and Wu, Jiajun and Tenenbaum, Joshua B, *End-to-end optimization of scene layout*, Proceedings of the IEEE/CVF Conference on Computer Vision and Pattern Recognition, 3754–3763, 2020. 1, 3
- [19] Dhano, Helisa and Manhardt, Fabian and Navab, Nassir and Tombari, Federico, *Graph-to-3d: End-to-end generation and manipulation of 3d scenes using scene graphs*, Proceedings of the IEEE/CVF International Conference on Computer Vision, 16352–16361, 2021. 1, 3, 7, 9, 10, 12, 13
- [20] Zhai, Guangyao and Örnek, Evin Pinar and Wu, Shun-Cheng and Di, Yan and Tombari, Federico and Navab, Nassir and Busam, Benjamin, *Commonscenes: Generating commonsense 3d indoor scenes with scene graphs*, Advances in Neural Information Processing Systems, 36, 2023. 1, 2, 3, 7, 8, 9, 10, 11, 12, 13, 14
- [21] Zhai, Guangyao and Örnek, Evin Pinar and Chen, Dave Zhenyu and Liao, Ruotong and Di, Yan and Navab, Nassir and Tombari, Federico and Busam, Benjamin, *EchoScene: Indoor Scene Generation via Information Echo over Scene Graph Diffusion*, European Conference on Computer Vision, 2024. 1
- [22] Ma, Yue and He, Yingqing and Cun, Xiaodong and Wang, Xintao and Chen, Siran and Li, Xiu and Chen, Qifeng, *Follow your pose: Pose-guided text-to-video generation using pose-free videos*, Proceedings of the AAAI Conference on Artificial Intelligence, 2024. 2
- [23] Wang, Zhouxia and Yuan, Ziyang and Wang, Xintao and Li, Yaowei and Chen, Tianshui and Xia, Menghan and Luo, Ping and Shan, Ying, *Motionctrl: A unified and flexible motion controller for video generation*, ACM SIGGRAPH Conference Papers, 2024. 2
- [24] Ben Mildenhall and Pratul P. Srinivasan and Matthew Tancik and Jonathan T. Barron and Ravi Ramamoorthi and Ren Ng, *NeRF: Representing Scenes as Neural Radiance Fields for View Synthesis*, European Conference on Computer Vision, 2020. 2
- [25] Zou, Zi-Xin and Yu, Zhipeng and Guo, Yuan-Chen and Li, Yangguang and Liang, Ding and Cao, Yan-Pei and Zhang, Song-Hai, *Triplane meets gaussian splatting: Fast and generalizable single-view 3d reconstruction with transformers*, Proceedings of the IEEE/CVF Conference on Computer Vision and Pattern Recognition, 2024. 2

- [26] Kim, Jaehyeon and Kong, Jungil and Son, Juhee, *Conditional variational autoencoder with adversarial learning for end-to-end text-to-speech*, International Conference on Machine Learning, 2021. [2](#)
- [27] Tan, Xu and Chen, Jiawei and Liu, Haohe and Cong, Jian and Zhang, Chen and Liu, Yanqing and Wang, Xi and Leng, Yichong and Yi, Yuanhao and He, Lei and Zhao, Sheng and Qin, Tao and Soong, Frank and Liu, Tie-Yan, *Naturalspeech: End-to-end text-to-speech synthesis with human-level quality*, IEEE transactions on pattern analysis and machine intelligence, 2024. [2](#)
- [28] Kerbl, Bernhard and Kopanas, Georgios and Leimkühler, Thomas and Drettakis, George, *3D Gaussian Splatting for Real-Time Radiance Field Rendering*, ACM Trans. Graph, 2023. [2](#)
- [29] Häne, Christian and Tulsiani, Shubham and Malik, Jitendra, *Hierarchical surface prediction for 3D object reconstruction*, International Conference on 3D Vision (3DV), 2017. [2](#)
- [30] Achlioptas, Panos and Diamanti, Olga and Mitliagkas, Ioannis and Guibas, Leonidas, *Learning representations and generative models for 3d point clouds*, International Conference on Machine Learning, 2018. [2](#)
- [31] Wang, Weiyue and Ceylan, Duygu and Mech, Radomir and Neumann, Ulrich, *3DN: 3D deformation network*, Proceedings of the IEEE/CVF Conference on Computer Vision and Pattern Recognition, 2019. [2](#)
- [32] Chen, Zhiqin and Zhang, Hao, *Learning implicit fields for generative shape modeling*, Proceedings of the IEEE/CVF conference on computer vision and pattern recognition, 2019. [2](#)
- [33] Su, Hang and Maji, Subhransu and Kalogerakis, Evangelos and Learned-Miller, Erik, *Multi-view convolutional neural networks for 3D shape recognition*, Proceedings of the IEEE International Conference on Computer Vision, 2015. [2](#)
- [34] Chang, Angel X and Funkhouser, Thomas and Guibas, Leonidas and Hanrahan, Pat and Huang, Qixing and Li, Zimo and Savarese, Silvio and Savva, Manolis and Song, Shuran and Su, Hao and others, *Shapenet: An information-rich 3d model repository*, arXiv preprint arXiv:1512.03012, 2015. [3](#)
- [35] Fu, Huan and Jia, Rongfei and Gao, Lin and Gong, Mingming and Zhao, Binqiang and Maybank, Steve and Tao, Dacheng, *3D-future: 3D furniture shape with texture*, International Journal of Computer Vision, 2021. [3](#), [8](#)
- [36] Deitke, Matt and Schwenk, Dustin and Salvador, Jordi and Weihs, Luca and Michel, Oscar and Vanderbilt, Eli and Schmidt, Ludwig and Ehsani, Kiana and Kembhavi, Aniruddha and Farhadi, Ali, *Objaverse: A universe of annotated 3D objects*, Proceedings of the IEEE/CVF Conference on Computer Vision and Pattern Recognition, 2023. [3](#), [14](#)
- [37] Deitke, Matt and Liu, Ruoshi and Wallingford, Matthew and Ngo, Huong and Michel, Oscar and Kusupati, Aditya and Fan, Alan and Laforte, Christian and Voleti, Vikram and Gadre, Samir Yitzhak and others, *Objaverse-xl: A universe of 10m+ 3d objects*, Advances in Neural Information Processing Systems, 36, 2024. [3](#), [14](#)
- [38] Paschalidou, Despoina and Kar, Amlan and Shugrina, Maria and Kreis, Karsten and Geiger, Andreas and Fidler, Sanja, *Atiss: Autoregressive transformers for indoor scene synthesis*, Advances in Neural Information Processing Systems, 2021. [3](#)
- [39] Subhabrata Mukherjee and Arindam Mitra and Ganesh Jawahar and Sahaj Agarwal and Hamid Palangi and Ahmed Awadallah, *Orca: Progressive Learning from Complex Explanation Traces of GPT-4*, arXiv 2306.02707, 2023. [3](#)
- [40] Haotian Liu and Chunyuan Li and Qingyang Wu and Yong Jae Lee and Jianwei Yang and Yong Zhang and Houdong Hu and Zicheng Liu and Jianfeng Gao, *Visual Instruction Tuning*, arXiv 2304.08485, 2023. [3](#)
- [41] Mu Cai and Yixiao Ge and Zhuohan Li and Zijian Wang and Yikang Shen and Demi Guo and Yiming Cui and Bin Zhao and Hao Zhang and Jianfeng Wang and Yizhou Wang, *Making Large Multimodal Models Understand Arbitrary Visual Prompts*, arXiv 2312.00784, 2023. [3](#)
- [42] Deyao Zhu and Jun Chen and Xiaoqian Shen and Xiang Li and Mohamed Elhoseiny, *MiniGPT-4: Enhancing Vision-Language Understanding with Advanced Large Language Models*, arXiv 2304.10592, 2023. [3](#)
- [43] Wang, Xueyang and Zeng, Xiangteng and Ghadirzadeh, Ali and Yin, Yue and Darrell, Trevor and Finn, Chelsea, *MAXI: Multi-Axis Instructional Videos*, Proceedings of the IEEE/CVF Conference on Computer Vision and Pattern Recognition, 22704–22714, 2022. [3](#)
- [44] Yan, Xinyu and Hu, Yuxiao and Zhao, Peiyu and Zhu, Xiaojun and Guo, Yaguang and Wang, Zihao and Xu, Changqing and Tao, Dacheng and Shen, Zheng and Geng, Xinwei and others, *InternVideo: General Video Foundation Models via Generative and Discriminative Learning*, arXiv preprint arXiv:2212.03191, 2022. [3](#)
- [45] Kukleva, Anna and Kuehne, Hilde and Sener, Fadime and Gall, Juergen, *HowToCaption: Prompting LLMs to Transform Video Annotations at Scale*, arXiv preprint arXiv:2310.04900, 2023. [3](#)
- [46] Tang, Jiapeng and Nie, Yinyu and Markhasin, Lev and Dai, Angela and Thies, Justus and Nießner, Matthias, *Diffuscene: Denoising diffusion models for generative indoor scene synthesis*, Proceedings of IEEE/CVF conference on computer vision and pattern recognition, 2024. [3](#)
- [47] Lin, Chenguo and Mu, Yadong, *Instructscene: Instruction-driven 3d indoor scene synthesis with semantic graph prior*, International Conference on Learning Representations, 2024. [3](#)
- [48] Feng, Weixi and Zhu, Wanrong and Fu, Tsu-jui and Jampani, Varun and Akula, Arjun and He, Xuehai and Basu, Sugato and Wang, Xin Eric and Wang, William Yang, *Layoutgpt: Compositional visual planning and generation with large language models*, Advances in Neural Information Processing Systems, 2024. [3](#)
- [49] Bahmani, Sherwin and Park, Jeong Joon and Paschalidou, Despoina and Yan, Xingguang and Wetzstein, Gordon and Guibas, Leonidas and Tagliasacchi, Andrea, *CC3D: Layout-conditioned generation of compositional 3D scenes*, Proceedings of the IEEE/CVF International Conference on Computer Vision, 2023. [3](#)
- [50] Gao, Gege and Liu, Weiyang and Chen, Anpei and Geiger, Andreas and Schölkopf, Bernhard, *Graphdreamer: Compositional 3d scene synthesis from scene graphs*, Proceedings of the IEEE/CVF Conference on Computer Vision and Pattern Recognition, 2024. [3](#)
- [51] Radford, Alec and Kim, Jong Wook and Hallacy, Chris and Ramesh, Aditya and Goh, Gabriel and Agarwal, Sandhini and Sastry, Girish and Askell, Amanda and Mishkin, Pamela and Clark, Jack and others, *Learning transferable visual models from natural language supervision*, International conference on machine learning, 8748–8763, 2021. [4](#)
- [52] Su, Hongjin and Shi, Weijia and Kasai, Jungo and Wang, Yizhong and Hu, Yushi and Ostendorf, Mari and Yih, Wen-tau and Smith, Noah A and Zettlemoyer, Luke and Yu, Tao, *One embedder, any task: Instruction-finetuned text embeddings*, arXiv preprint arXiv:2212.09741, 2022. [4](#)
- [53] Curless, Brian and Levoy, Marc, *A volumetric method for building complex models from range images*, Proceedings of the 23rd annual conference on Computer graphics and interactive techniques, 303–312, 1996. [5](#)
- [54] Van Den Oord, Aaron and Vinyals, Oriol and others, *Neural discrete representation learning*, Advances in neural information processing systems, 30, 2017. [5](#)
- [55] Çiçek, Özgün and Abdulkadir, Ahmed and Lienkamp, Soeren S and Brox, Thomas and Ronneberger, Olaf, *3D U-Net: learning dense volumetric segmentation from sparse annotation*, Medical Image Computing and Computer-Assisted Intervention–MICCAI 2016: 19th International Conference, Athens, Greece, October 17–21, 2016, Proceedings, Part II 19, Springer, 424–432, 2016. [6](#)
- [56] Fu, Huan and Cai, Bowen and Gao, Lin and Zhang, Ling-Xiao and Wang, Jiaming and Li, Cao and Zeng, Qixun and Sun, Chengyue and Jia, Rongfei and Zhao, Binqiang and others, *3d-front: 3d furnished rooms with layouts and semantics*, Proceedings of the IEEE/CVF International Conference on Computer Vision, 10933–10942, 2021. [8](#)
- [57] Heusel, Martin and Ramsauer, Hubert and Unterthiner, Thomas and Nessler, Bernhard and Hochreiter, Sepp, *Gans trained by a two time-scale update rule converge to a local nash equilibrium*, Conference on Neural Information Processing Systems, 30, 2017. [8](#)
- [58] Bińkowski, Mikołaj and Sutherland, Danica J and Arbel, Michael and Gretton, Arthur, *Demystifying mmd gans*, International Conference on Learning Representations, 2018. [8](#)
- [59] Fan, Haoqiang and Su, Hao and Guibas, Leonidas J, *A point set generation network for 3d object reconstruction from a single image*, Proceedings of the IEEE conference on computer vision and pattern recognition, 605–613, 2017. [8](#)
- [60] Yang, Guandao and Huang, Xun and Hao, Zekun and Liu, Ming-Yu and Belongie, Serge and Hariharan, Bharath, *Pointflow: 3d point cloud generation with continuous normalizing flows*, Proceedings of the IEEE/CVF international conference on computer vision, 4541–4550, 2019. [8](#)
- [61] Ilya Loshchilov and Frank Hutter, *Decoupled Weight Decay Regularization*, International Conference on Learning Representations, 2019. [8](#)

- [62] Chen, Dave Zhenyu and Li, Haoxuan and Lee, Hsin-Ying and Tulyakov, Sergey and Nießner, Matthias, *Scenetex: High-quality texture synthesis for indoor scenes via diffusion priors*, Proceedings of the IEEE/CVF Conference on Computer Vision and Pattern Recognition, 2024. 13
- [63] Tang, Shitao and Zhang, Fuyang and Chen, Jiacheng and Wang, Peng and Furukawa, Yasutaka, *MVDiffusion: Enabling Holistic Multi-view Image Generation with Correspondence-Aware Diffusion*, arXiv preprint arXiv:2307.01097, 2023. 13
- [64] Chen, Zhaoxi and Wang, Guangcong and Liu, Ziwei, *Scenedreamer: Unbounded 3d scene generation from 2d image collections*, IEEE transactions on pattern analysis and machine intelligence, 2023. 14
- [65] Lee, Jumin and Lee, Sebin and Jo, Changho and Im, Woobin and Seon, Juhyeong and Yoon, Sung-Eui, *SemCity: Semantic Scene Generation with Triplane Diffusion*, Proceedings of the IEEE/CVF Conference on Computer Vision and Pattern Recognition, 2024. 14
- [66] Ouyang, Long and Wu, Jeffrey and Jiang, Xu and Almeida, Diogo and Wainwright, Carroll and Mishkin, Pamela and Zhang, Chong and Agarwal, Sandhini and Slama, Katarina and Ray, Alex and others, *Training language models to follow instructions with human feedback*, Advances in neural information processing systems, 35, 2022. 14
- [67] OpenAI, *GPT-4 Technical Report*, arXiv preprint arXiv:2303.08774, 2023. 14
- [68] Touvron, Hugo and Lavril, Thibaut and Izacard, Gautier and Martinet, Xavier and Lachaux, Marie-Anne and Lacroix, Timothée and Rozière, Baptiste and Goyal, Naman and Hambro, Eric and Azhar, Faisal and others, *Llama: Open and efficient foundation language models*, arXiv preprint arXiv:2302.13971, 2023. 14